AIAA JOURNAL
Vol. 50, No. 10, October 2012

Measurements of Aerodynamic Coefficients for Flapping Wings at 0–90 Angles of Attack

Sergey Shkarayev* and Dmytro Silin†
University of Arizona, Tucson, Arizona 85721

DOI: 10.2514/1.J051051

This paper addresses the aerodynamics of membrane flapping wings. In a series of wind-tunnel experiments on the 25 and 74-cm-wingspan models, the stroke-averaged lift and horizontal force were measured at an angle of attack that varied from 0 deg (horizontal) to 90 deg (hovering position). The flapping frequency was held constant, and freestream velocity was varied with the advance ratio range 0–1.2. For high angles of attack, flapping wings do not exhibit a typical abrupt stall seen with fixed wings. This feature in flapping wings allows a smooth transition from a level flight to hovering and back. The angle of attack, corresponding to a balance of forces in the horizontal direction, decreases exponentially with advance ratio. Aerodynamic coefficients are defined using a reference velocity as a vector sum of a freestream velocity and a stroke-averaged wing-tip flapping velocity. The lift and drag coefficients obtained using this procedure collapse well for the studied advance ratios, especially at lower angles of attack. Polynomial approximations for aerodynamic coefficients are proposed that can be used in flight-performance analysis.

Nomenclature

A	=	partial disk area
a	=	chord
B	=	$\beta_{\max} - \beta_{\min}$, amplitude of angle of incidence
b	=	$2R$, wingspan
C_D	=	drag coefficient
C_L	=	lift coefficient
C_T	=	thrust coefficient
c	=	coefficient of variation
D	=	drag force
f	=	flapping frequency
J	=	advance ratio
K	=	empirical constant
k	=	empirical constant
L	=	lift force
l	=	spacing of battens
R	=	wing length
Re	=	Reynolds number based on mean aerodynamic chord and vector sum of stroke-averaged wing-tip velocity and freestream velocity
S	=	wing area
T	=	thrust force
V	=	freestream velocity
V_T	=	stroke-averaged wing-tip speed
w	=	induced velocity
X	=	horizontal force
α	=	angle of attack of flapping wing
α_b	=	balanced angle of attack
β	=	angle of incidence of flapping wing
γ	=	angle of batten
μ	=	mean value
ν	=	air kinematic viscosity
ρ	=	air density
σ	=	standard deviation
Φ	=	$\varphi_{\max} - \varphi_{\min}$, amplitude of flapping angle
φ	=	flapping angle

Subscripts

0	=	refers to test conditions without freestream ($V = 0$)
c	=	characteristic velocity
m	=	index
mg	=	mean geometric
r	=	wing root
λ	=	$\{C_L, C_D\}$, index

Presented at the 47th AIAA Aerospace Sciences Meeting, Orlando, Florida, January 5–8, 2009; received 4 November 2010; revision received 28 March 2012; accepted for publication 15 April 2012.

*Professor, Department of Aerospace and Mechanical Engineering, 1130 North Mountain Avenue. Senior Member AIAA.

†Graduate Research Assistant, Department of Aerospace and Mechanical Engineering, 130 North Mountain Avenue.

I. Introduction

FLAPPING-WING micro air vehicles (ornithopters) generate lift for staying airborne and thrust for forward motion by emulating birds and insects. However, just mimicking the flight of birds and insects may not be sufficient for designing ornithopters. Following is how this viewpoint was elucidated by Mueller and DeLaurier (p. 7) [1]: "The primary motivation for studying animal flight is to explain the physics for a creature that is known to fly. An ornithopter designer, in contrast, is trying to develop a flying aircraft, and its ability to achieve this is no given fact." On the other hand, a successful micro air vehicle design can provide a verifiable physical model of flight in nature.

AeroVironment, Inc., pioneered the designing of radio-controlled micro ornithopters [2]. Their most successful vehicle has a half-ellipse wing planform with a 20 cm wingspan and flapping frequency of 22 Hz.

DeLaurier [3] developed a 35 cm ornithopter capable of hovering. A clap-and-fling mechanism for enhancing the lift was employed using a four-wing transmission design. Hovering flights in excess of 1 min were achieved at a flapping frequency of 28 Hz. It was noted that transition from hover to forward flight remains a problem for this type of vehicle.

The University of Arizona has developed several successful ornithopters. The smallest ornithopter (Fig. 1a) weighs only 9 g and uses membrane battened wings with a 15 cm wingspan. This ornithopter can fly for more than 3 min at a speed from 1 m/s to 5 m/s.

The flight dynamics of a larger ornithopter with a 74 cm wingspan (Fig. 1b) was investigated in our previous work [4] using a vehicle equipped with an autopilot. Essential stability parameters and basic dynamic modes were investigated through extensive wind-tunnel

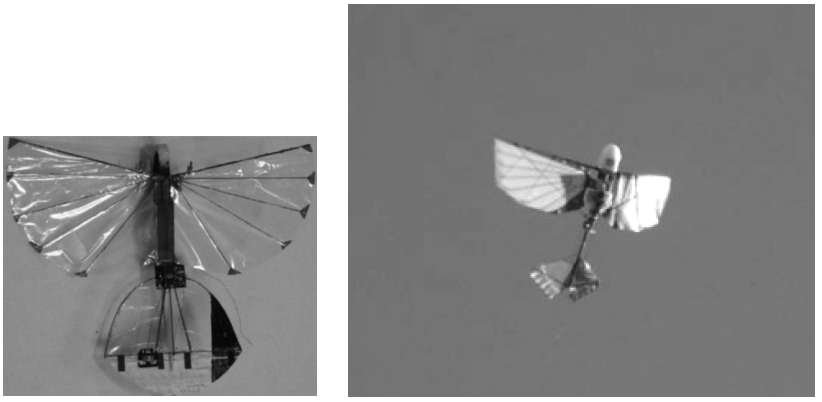

a) 15 cm wingspan **b) 74 cm wingspan**

Fig. 1 University of Arizona ornithopters.

and flight measurements. In a series of autonomous and control-fixed flights, active controls and passive aerodynamic stability of the flapping-wing apparatus were demonstrated. These experiments showed the existence of a similar type of low-frequency oscillatory dynamics in both roll and pitch motions of the ornithopter. This work also suggested that systematic studies on the aerodynamics of membrane flapping wings are needed to better understand the flight dynamics of flapping-wing vehicles.

Motion of membrane flapping wings includes articulated rotations at their base as well as elastic deformations. Because the aerodynamic center of pressure, center of mass, and shear center do not typically coincide in these wings, resultant forces and moments cause wings to twist (chordwise bending). Thus, a spanwise change of the angle of incidence is achieved through partially active and partially passive twisting deformations of the wing structure.

There are several underlying physics phenomena in the aerodynamics of flapping wings: leading-edge vortex, wake capture, near fling, and apparent mass. Results of recent experimental and theoretical investigations of flapping flight were covered in reviews underlying fluid mechanics and aerodynamics [5–7], flapping-flight controls [8], and theoretical and numerical modeling [9,10]. All of these studies found it difficult to explain aerodynamic effects of structural deformations in the membrane flapping wings.

It is worth mentioning the difficulties involved in obtaining direct measurements of cyclic aerodynamic forces in flying animals and the consequent difficulties of experimental validation of proposed theories. In contrast, man-made membrane wings represent a useful model for the study of the aerodynamics of flapping flight. Two types of wing models have been investigated in previous studies: rigid and membrane. Time-varying pitching of rigid wings is realized with the help of an articulated pitching mechanism. Flapping membrane wings feature a leading edge spar that actuates the flapping motion. A flexible membrane attached to the spar is twisted during the flapping cycle, providing wing pitch.

Van den Berg and Ellington [11] developed a 10:1 scale model mimicking the flapping motion of the hawkmoth *Manduca sexta*. Using flow visualization of airflow around the wings during the downstroke, vortices were found to form along the leading edge, which moved toward the wing tip with its diameter increased, becoming unstable and detached from the wing's surface at about 75% radial distance of the wing. The vortex diameter was smaller than predicted for linearly translating wings. The leading edge vortex joined the tip vortex and the combined starting/stopping vortex. Thus, at the end of the downstroke, the wake had the form of a ring. Performed analysis showed that a sufficient lift was produced for the moth's weight support.

Van den Berg and Ellington [12] further analyzed results of their study [11] to identify a mechanism responsible for the generation of the leading edge vortex. Two hypotheses were considered: dynamic stall during the translation phase of flapping and the wing's rotation during up- and downstrokes. The leading edge vortex was clearly observed [11] throughout a translation; therefore, dynamic stall was suggested as the main mechanism for the creation of the vortex. Its stabilization in the spanwise direction was explained by a strong axial flow from the root to the tip of the flapping wing. It was pointed out that this unsteady aerodynamic mechanism is analogous to leading edge vortices observed in delta wings.

Dickinson [13] and Dickinson et al. [14] investigated rigid translating–rotating wings. They constructed a scaled model of fruit fly wings, immersed them in mineral oil, and measured instantaneous forces on the wings directly. The authors suggested that rotational circulation and wake capture are unsteady mechanisms contributing to aerodynamic force generation in flapping wings during pronation and supination.

Designing a small-scale flapping-pitching mechanism is not a simple problem, and mechanical design drawbacks can prevent one from obtaining accurate data. Singh and Chopra [15] studied the performance of flapping wings in still air. Their flapping-wing model employs an articulated flapping and pitching mechanism. Static thrust and mechanical power were measured for varied flapping frequencies, pitching angles, and wing designs. Two flapping-pitching mechanisms were built: a bistable pitching device and a passive device using a torsion spring. An aluminum frame and composite frame wings were tested on both pitching setups. Higher thrust was obtained with the aluminum frame wing than with the composite wing on the bistable pitch mechanism. However, when the wings were tested on the passive pitching setup, the resulting forces changed dramatically. Reasons for this change remain unclear.

One key element in the production of aerodynamic forces by flapping wings lies in the flexibility of the wing structure, which has to be accounted for. Gallivan and DeLaurier [16] conducted experimental studies of membrane flapping wings in a wind tunnel. Lift, thrust, and pitching moment were measured and averaged over a flapping cycle. Significant scatters in the data were explained by a zero drift in the strain-gage balance. Effects of geometrical, mass, and stiffness parameters of membrane wings were investigated and discussed. It was shown that stiffening the front spar increased the thrust and had negligible effect on lift. The presence of full chord-length battens showed a positive effect on both lift and thrust forces. However, measurements were performed for only two values of angle of attack of 0 and 10 deg.

Effects of wing size, advance ratio, and variations of angle of attack from horizontal to vertical (hovering position) have not been investigated thoroughly in membrane flapping wings. These problems will be addressed in the present study.

The aerodynamic forces can be nondimensionalized by using a set of independent dimensional parameters of the air flowfield. These parameters normally are: characteristic time scale, characteristic length scale, and characteristic velocity scale. A flapping cycle period represents the characteristic time scale, and it is used in the averaging of forces over the flapping period in the presented experiments. The length scale is either a wing length or a chord.

There is more than one candidate for the characteristic velocity in flapping flight. For a hover, a theoretical wing-tip velocity was used

in previous studies [10,17,18]. Forward flight with a relatively high speed is another limiting case for which a freestream velocity can be chosen as the characteristic one. However, using two dissimilar sets of parameters for the characterization of flapping-wing aerodynamics is not a convenient approach. Study [19] has emphasized the importance of the selection of a characteristic velocity that will combine all phases of flight.

The objectives of the present study are to investigate the essential aerodynamic characteristics of flapping wings featuring a flexible membrane attached to a spar and stiffened by battens. In this study, wind-tunnel measurements of stroke-averaged aerodynamic forces were conducted, and several effects were investigated, including wing size, advance ratio, and variation of the angle of attack from horizontal to vertical. The problem of the selection of a characteristic velocity is analyzed based on the experimental data generated in this study. The thrust, lift, and drag coefficients were defined using a vector sum of a freestream velocity and mean flapping velocity of the wing tip.

II. Experimental Setup

A. Wind-Tunnel Facility

Experimental studies were performed in the University of Arizona Wind Tunnel. This wind tunnel has a 3×4 ft test section, and in the present study it was operated in the velocity range from 2 to 9 m/s. The flow is laminarized in a settling chamber to less than 0.3% turbulence in the axial direction. More details on this wind tunnel can be found in [20].

An external aerodynamic force balance was used in the study to record lift and drag forces. Data from strain gages were collected using two National Instruments SCXI-1321 terminal blocks in a low-noise SCXI-1000 chassis capable of sampling at 330,000 Hz. The resolution of each flexure was about 0.004 N. The zero drift for flexures did not exceed 1.5% over 15 min of test time with no load applied. When an oscillatory load was applied through the 25 cm flapping wings operating at 20 Hz, the zero drift for the same flexures did not exceed 2% per 15 min of test run. Calibration of the wind tunnel and the balance was performed before each test series.

The uncertainty intervals in aerodynamic forces corresponding to a confidence level of 90% were determined. For the range of measured forces (0–5 N), the uncertainty intervals were 0.015 N for vertical and 0.007 N for horizontal forces. The value of the lift channel uncertainty was higher because the lift was measured by two flexures; thus, two sources of measurement errors contributed to the total uncertainty. For the pitching moment of order 0–0.15 N · m, the uncertainty interval was of 0.0005 N · m. The standard deviation of measured dynamic pressure was 0.4 N/m^2 for the range of velocities studied in the present work.

B. Flapping-Wing Models

Aerodynamic force measurements were conducted for two flapping-wing models with wingspans of 25 and 74 cm (Fig. 2). Each test subject consisted of a DC motor, mounting rib, flapping wing, and transmission. Generic drawings are shown in Fig. 3. Geometrical, kinematic, and mass data for both wings are presented in Table 1.

The 25 cm wing structure consisted of wing arms, front spar, four battens, and membrane. Wing arms were made of 0.8 mm music wire. The membrane was 0.015 mm Mylar bonded to the front spar and battens with rubber cement. Pultruded carbon rods were used: T315-4 of diameter 0.8 mm for the front spar and T305-4 of diameter 0.5 mm for battens. Battens were not rigidly fixed to the front spar, allowing pitching deformations of the membrane caused by inertia and aerodynamic forces.

A wing from a commercial ornithopter, Cybird P2, was used as the 74 cm flapping-wing model. Its structure included front and rear spars, six battens, and membrane made of nylon cloth. Battens were rigidly fixed to both front and rear spars.

25 cm flapping wing

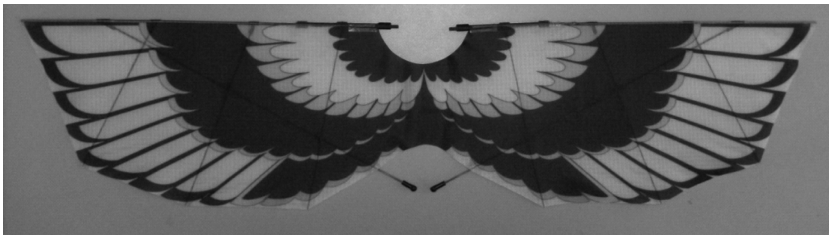

74 cm flapping wing

Fig. 2 Flapping wings studied.

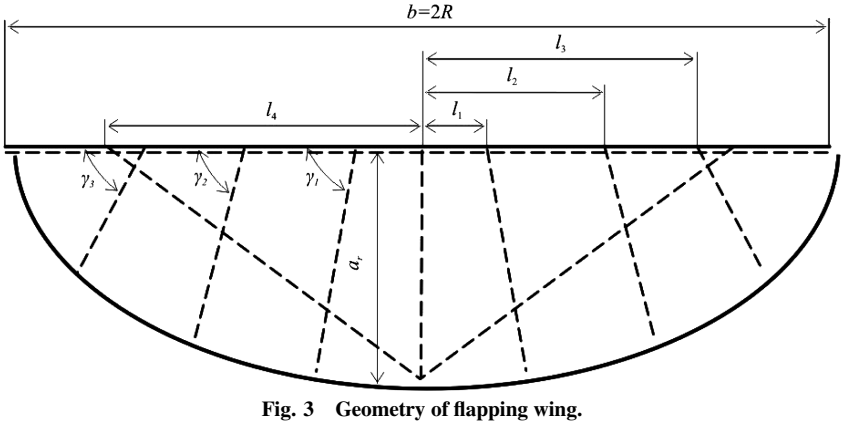

Fig. 3 Geometry of flapping wing.

Table 1 Specifications of flapping-wing models

Wing model	25 cm	74 cm
Wingspan b, cm	25	74
Flapping frequency f, Hz	22	9.2
Flapping angle amplitude Φ, deg	66	55
Angle of incidence amplitude B, deg	146	95
Wing area S, cm^2	137	991
Batten 1 $l_1 \times \gamma_1$, cm × deg	3.8 × 77	7.5 × 80
Batten 2 $l_2 \times \gamma_2$, cm × deg	7.8 × 70	15.5 × 70
Batten 3 $l_3 \times \gamma_3$, cm × deg	-	24.0 × 65
Intersection point l_4, cm	-	27
Root chord a_r, cm	7	16.8
Wing-tip deflection cm/g	0.18	0.95
Mass, g	1.15	15.8

For the flapping frequency measurements, the experimental setup was equipped with a built-in optical tachometer. The tachometer consisted of a CP-36 photodiode and ECG-3038 phototransistor connected to the data-acquisition board.

Conventions used for flapping angle φ and angle of incidence β are illustrated in Fig. 4a. The orientation of a flapping-wing model with respect to a freestream is described by the angle of attack of the flapping wing, α, which is defined as the angle between the flapping axis (x_φ axis in Fig. 4a) and the freestream direction (x axis in Fig. 4a). The $x_\varphi y_\varphi z_\varphi$ coordinate system is a rotating frame about the flapping axis x_φ.

High-speed videography was used in measuring kinematic parameters of the 74 cm [Vicon Nexus Video, 500 frames per second (fps)] and 25 cm (Phantom 7.1 cameras, 1000 fps) flapping wings [21,22]. Experiments were conducted in free flights and on the ground. Data of high spatial and time resolution were obtained and presented in [21,22] for time-varying flapping angles, angles of incidence, and front spar and camber deformations. Values for flapping angle amplitudes Φ, determined at the wing base, and angle of incidence amplitudes B, determined at batten 2, are given in Table 1 for bench-top experiment cases.

The aerodynamic forces $L = L(\alpha, J)$ and $X = X(\alpha, J)$ were determined in the wind-tunnel frame of reference, as shown in Fig. 4b.

Table 2 Test freestream velocities V, m/s

Wing model	J				
	0.4	0.6	0.8	1	1.2
25 cm	2.77	4.15	5.53	6.94	8.30
74 cm	2.61	3.92	5.23	6.54	7.84

III. Aerodynamic Forces

The flapping-wing models were tested in the wind tunnel at an angle of attack varying from the horizontal ($\alpha = 0$ deg) to the vertical position ($\alpha = 90$ deg) in increments of 1.22 deg per data point.

Assuming a sinusoidal flapping motion, the stroke-averaged wing-tip speed is $V_T = 2R\Phi f$, and so the advance ratio is defined as

$$J = \frac{V}{V_T} = \frac{V}{2R\Phi f} \tag{1}$$

The advance ratio was varied in the range from 0.4 to 1.2. This was achieved by varying the freestream velocity V for flapping frequencies f held constant at 22 and 9.2 Hz for 25 and 74 cm wings, respectively. Corresponding values of freestream velocities used in the experiments are presented in Table 2.

The results of measurements for the stroke-averaged lift forces are presented in Figs. 5 and 6 for 74 and 25 cm wings, respectively. The data are less scattered for the 74 cm wing, which can be explained by higher magnitudes of measured forces for this model. Even though the wings are nominally flat and flap symmetrically, nonzero lift forces were observed at $\alpha = 0$ deg. These can be explained by some nonsymmetry in flapping transmission and the geometrical and stiffness properties of the flapping-wing models.

Overall, the plots exhibit similar trends and nonlinear behaviors at higher angles of attack. The maximum forces for the 74 cm wing are 5.8–6.4 times greater than for the 25 cm wing and are comparable to the ratio of these wings' areas of 7.2.

After reaching maxima, lift slowly decreases. It appears that, as the freestream velocity increases (J increases), the lift increases. It is noted from Figs. 5 and 6 that the flapping wings do not exhibit

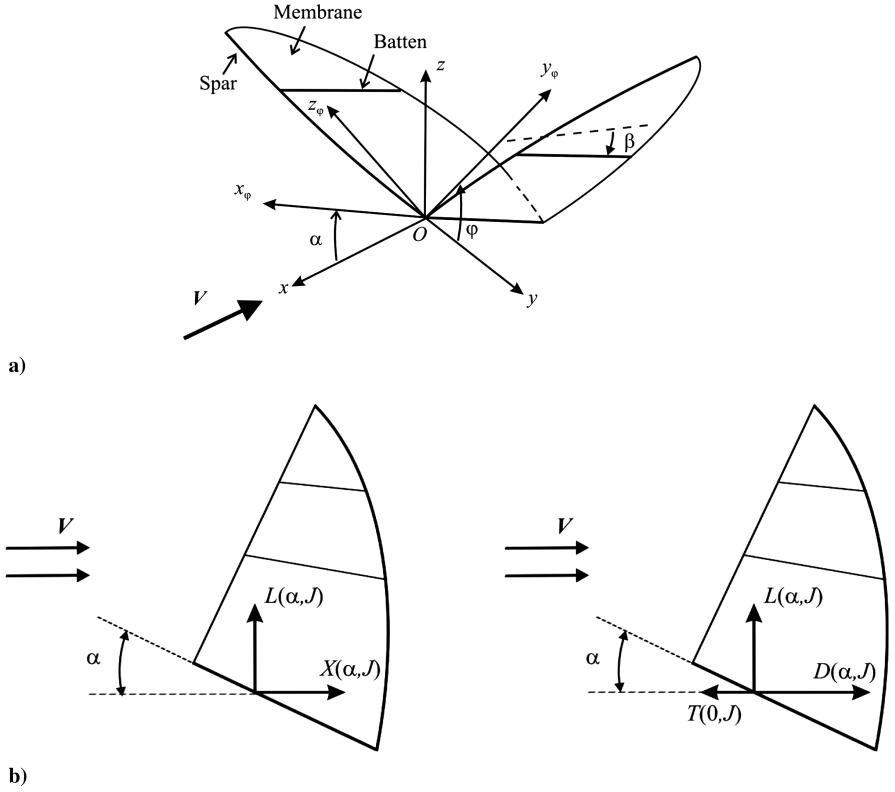

Fig. 4 Conventions used for a) angles and b) positive forces.

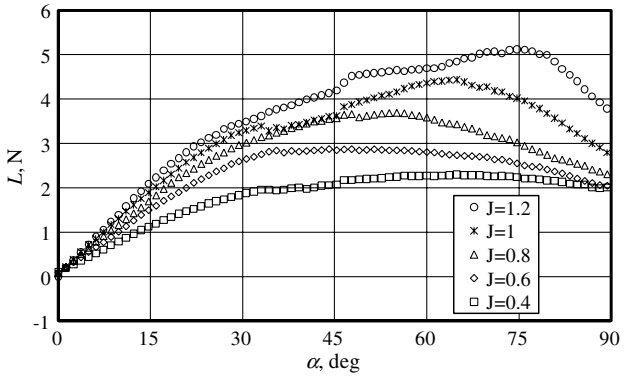

Fig. 5 Variation of lift force with angle of attack and advance ratio (74 cm wing).

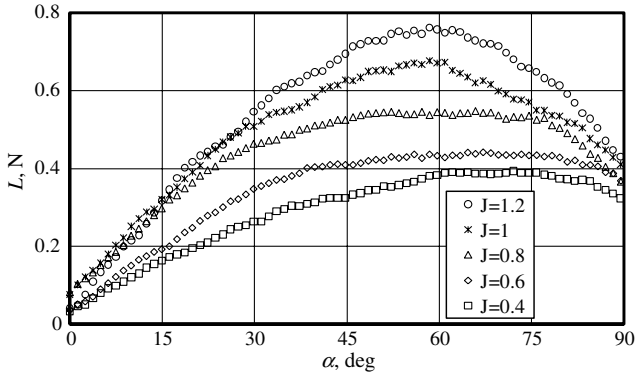

Fig. 6 Variation of lift force with angle of attack and advance ratio (25 cm wing).

the typical abrupt stall seen with the fixed wings. The mechanism of nonstalling in flapping wings can be partially explained by considering dynamic pressure changes during advancing and retreating strokes. During advancing stroke (against the wind), the freestream speed is added to the flapping speed, whereas on the retreating stroke (with the wind) the freestream speed is subtracted from the flapping speed (see Fig. 7). Thus, a nonstalling mechanism in flapping wings makes use of the higher dynamic pressure on the advancing stroke that prevails over the lower dynamic pressure on the retreating stroke.

Note that, as J increases, the lift $L(\alpha = 90 \text{ deg}, J)$ increases, and it is higher than the propulsive thrust at zero speed. This increase of the lift confirms the results of our previous study [23]. Experimental results of the work [23] were also in satisfactory agreement with Glauert's [24] disk-actuator theory for relatively low freestream velocities. These features of flapping-wing aerodynamics have significant implications for the performance of flapping-wing vehicles. The smoothness of the lift curve for the whole range of the angle of attack from the horizontal ($\alpha = 0$ deg) to the vertical position ($\alpha = 90$ deg) is necessary for providing a smooth transition from a level flight to a hover and back. In a case of increased flight speed or if a wind gust hits a flapping-wing vehicle in a hover, the lift generated by flapping wings increases. This will push a flapping-wing air vehicle upward from the ground, which is a safe passive response to a gust. Certainly, additional experiments are needed to determine precisely a wing's transient response to a gust of a specific profile.

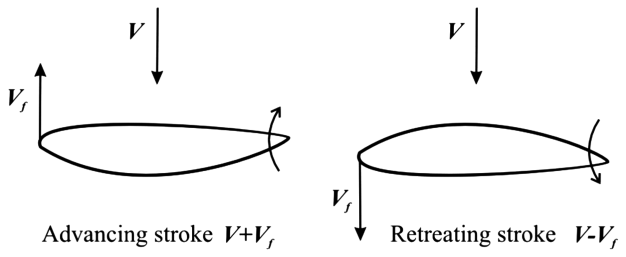

Fig. 7 Total airspeed during advancing and retreating strokes for flapping wings in a vertical position.

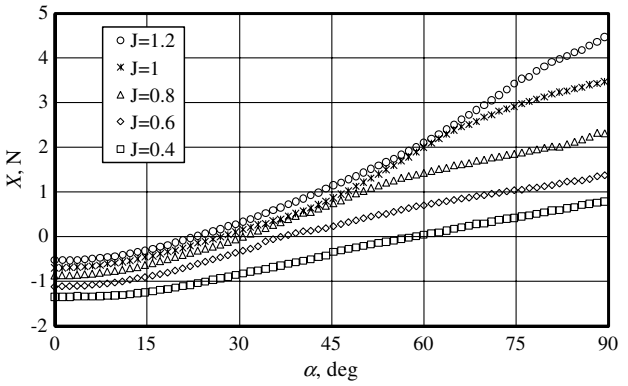

Fig. 8 Variation of horizontal force with angle of attack and advance ratio (74 cm wing).

Similarly to fixed wings, the horizontal force plots for flapping wings in Figs. 8 and 9 are concave. Its magnitude increases with an increase of the angle of attack and advance ratio. The horizontal force can be presented as the sum of two parts:

$$X(\alpha, J) = X(0, J) + D(\alpha, J) \tag{2}$$

Note that, in the performed tests, $X(0, J) < 0$; the first part represents a pointing-forward propulsive thrust force $T(\alpha = 0, J) = -X(0, J)$. The second part will be called the drag $D(\alpha, J)$ and can be found from

$$D(\alpha, J) = X(\alpha, J) - X(0, J) \tag{3}$$

The proposed decomposition of stroke-averaged horizontal force is illustrated in Fig. 4b. It is analogous with models used in conventional fixed-wing aircraft. Thus, methods of analysis of performance, flight dynamics, and controls of fixed-wing aircraft can be used in a flapping-wing apparatus.

The angle of attack α_b corresponding to $X = 0$ is an important parameter of air vehicle performance. It corresponds to the equilibrium of the thrust and the drag forces in a steady, level flight. It will be called a balanced angle. Experimental data points for α_b versus J are presented in Fig. 10 for both wings. As can be seen, both sets of data exhibit similar behaviors and are fairly close to each other. It points out the aerodynamic similarities of these two flapping wings.

The balanced angle α_b decreases with J exponentially. For a given J, the balanced angle is higher for the 74 cm wing. Clearly, for the hovering flight, $\alpha_b = 90$ deg at $J = 0$. Based on these observations, a useful approximation is proposed:

$$\alpha_b = 90e^{-KJ} \tag{4}$$

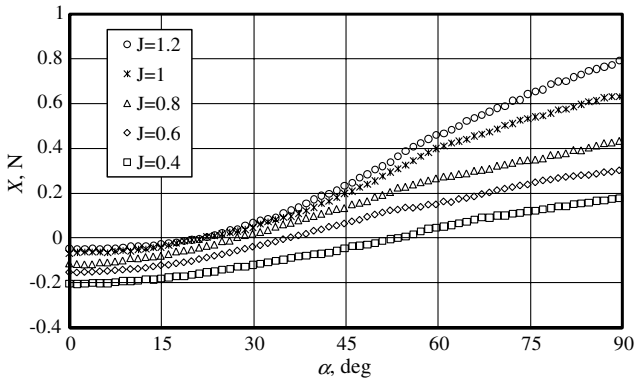

Fig. 9 Variation of horizontal force with angle of attack and advance ratio (25 cm wing).

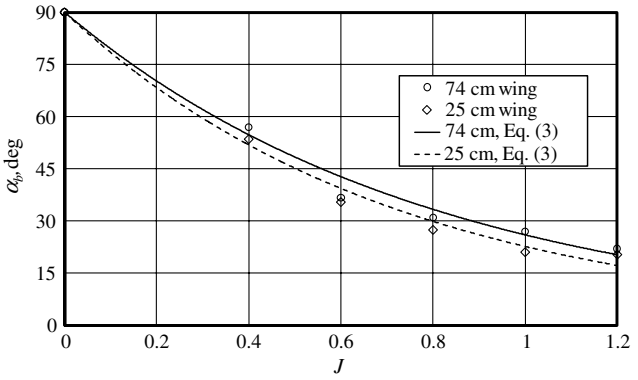

Fig. 10 Variation of balanced angle of attack with advance ratio.

Values of the constant K were determined using regression analysis: -1.38 and -1.24 for the 74 and 25 cm wings, respectively. As is evident from Fig. 10, Eq. (4) is in satisfactory agreement with the experimental data.

IV. Aerodynamic Force Coefficients

For the fixed wings, aerodynamic forces are nondimensionalized using for reference a wing area and a freestream dynamic pressure. However, these definitions, as well as the freestream velocity-based conventional definition of the Reynolds number (see discussion in Sec. I), will fail for the flapping wings in hovering flight; therefore, the freestream velocity alone cannot be chosen as a characteristic velocity. In the following discussion, the problem of selection of a characteristic velocity is addressed using the experimental data for aerodynamic forces obtained in the present study.

Here, Reynolds number, thrust, and lift coefficients are defined as

$$Re = \frac{a_{\text{mg}} V_C}{\nu} \tag{5}$$

$$C_T = \frac{T(0,J)}{0.5\rho V_C^2 S} \tag{6}$$

$$C_L = \frac{L(\alpha,J) - L(0,J)}{0.5\rho V_C^2 S} \tag{7}$$

and, using Eq. (3), the drag coefficient is defined as

$$C_D = \frac{X(\alpha,J) - X(0,J)}{0.5\rho V_C^2 S} \tag{8}$$

One possible choice for a characteristic velocity V_C is the geometric sum of a freestream velocity and a flapping velocity. If the maximum flapping-wing-tip velocity $V_{\max} = \pi R f \Phi$ is used, the characteristic velocity becomes

$$V_{C1} = \sqrt{V^2 + (\pi R f \Phi)^2} \tag{9}$$

Otherwise, if the stroke-averaged wing-tip velocity V_T is chosen, the characteristic velocity is

$$V_{C2} = \sqrt{V^2 + (2 R f \Phi)^2} \tag{10}$$

Application of the actuator-disk theory to a flapping flight [23] would be another resolution to the selection of the characteristic velocity. A correction to the hovering induced velocity was proposed by Ellington [25] as

$$w_{0C} = k w_0 = k\sqrt{\frac{T_0}{2\rho A}} \tag{11}$$

where k is the empirical correction factor, $A = \Phi b^2/4$ is the partial disk area, and T_0 is the thrust force corresponding to $V = 0$. Numerical values for the correction factor obtained in the previous study [23] are 1.81 and 2.68 for the 25 and 74 cm wings, respectively. For a forward flight at a given V and at zero angle of attack, the induced velocity is found from

$$w_C = -0.5V + \sqrt{0.25V^2 + w_{0C}^2 \frac{T}{T_0}} \tag{12}$$

A sum of forward velocity and the velocity induced in the flow passing the disk gives the characteristic velocity as

$$V_{C3} = V + w_C = 0.5V + \sqrt{0.25V^2 + w_{0C}^2 \frac{T}{T_0}} \tag{13}$$

Using the ultimate change of the velocity in the far wake of $2w_C$, the characteristic velocity can be written as

$$V_{C4} = V + 2w_C = \sqrt{V^2 + 4w_{0C}^2 \frac{T}{T_0}} \tag{14}$$

With four candidates proposed, one possible criterion for selection of the characteristic velocity would be a closeness of obtained experimental data presented in a form of aerodynamic coefficients C_L and C_D. Formally, the closeness of data for aerodynamic coefficients C_L and C_D across all investigated advance ratios J and angles of attack α can be assessed in terms of a coefficient of variation. For a given angle of attack α_m, a coefficient of variation $c_{\lambda m}$ for an aerodynamic coefficient $\lambda = \{C_L, C_D\}$ across $N = 5$ values of advance ratio can be found from

$$c_{\lambda m} = \frac{\sigma_\lambda(\alpha_m)}{\mu_\lambda(\alpha_m)} \tag{15}$$

where $\mu_\lambda(\alpha_m) = 1/N \sum_{i=1}^{N} \lambda_i$ and $\sigma_\lambda(\alpha_m) = \sqrt{1/N \sum_{i=1}^{N} (\lambda_i - \mu_\lambda)^2}$ are the mean value and the standard deviation, respectively. Further, these coefficients of variation can be averaged over $M = 73$ angles of attack

$$c_\lambda = \frac{1}{M} \sum_{m=1}^{M} c_{\lambda m} \tag{16}$$

providing a numerical parameter to quantify how well the aerodynamic coefficients data collapse across advance ratios and angles of attack.

Coefficients of variations were calculated for the 25 and 74 cm models and are presented in Table 3. Only data points corresponding to the forces above the balance resolution were used in calculations of c_λ. Thus, troublesome regions where mean values of C_D and C_L approach zero were avoided.

As is evident from the table, the characteristic velocity V_{C2} minimizes both c_{C_D} and c_{C_L} for both the 74 and 25 cm models. Also, V_{C2} is more practical than other candidates, because average wing-tip velocity could be determined easily from the measured stroke amplitude and flapping frequency. Based on this analysis, V_{C2} is chosen as a characteristic velocity in the present study.

Table 3 Coefficient of variations, c_λ, $\lambda = \{C_L, C_D\}$

Wing model	25 cm		74 cm	
λ	C_L	C_D	C_L	C_D
V_{C1}	0.107	0.137	0.156	0.156
V_{C2}	0.076	0.098	0.082	0.125
V_{C3}	0.236	0.312	0.100	0.195
V_{C4}	0.079	0.164	0.354	0.330

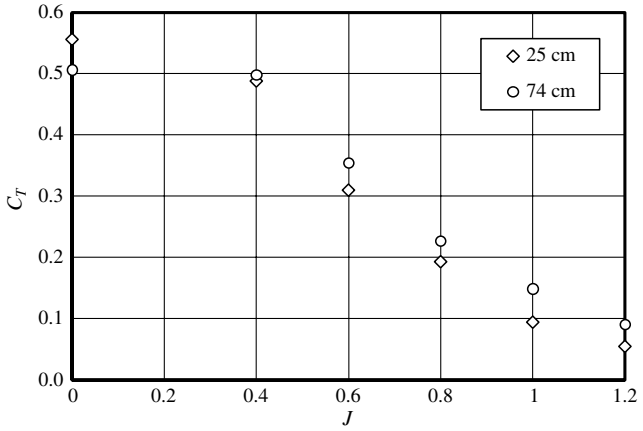

Fig. 11 Variation of thrust coefficient with J.

V. Discussions

In our previous study [23], experiments were conducted at zero freestream velocity ($J = 0$) with varying flapping frequencies. The values of measured thrust force are found [23] to be 0.205 and 1.346 N for the 22 Hz in 25 cm and 9.2 Hz in 74 cm wings, respectively. Using these values and data for the horizontal force component $T(J) = -X(\alpha = 0, J)$ at $\alpha = 0$ for $J = 0.4 \ldots 1.2$ (see Figs. 8 and 9), thrust coefficients are computed using Eq. (6) and shown in Fig. 11. The plot shows the variation of thrust coefficient with advance ratio. As expected, the thrust coefficient decreases with advance ratio. Coefficients for the two wings diverge from each other at higher J.

Using the aerodynamic forces data presented in Figs. 5, 6, 8, and 9, lift and drag coefficients were calculated with the help of Eqs. (7) and (8) and are presented in Figs. 12–17. Data collapse well, especially for lower angles of attack. Error bars in Figs. 16 and 17 corresponding to the 90% confidence were calculated based on uncertainties presented in Sec. II.A.

The lift coefficient curve is approximated by a quadratic function:

$$C_L = C_1\alpha + C_2\alpha^2 \tag{17}$$

The best fit in the least-squares sense was applied to minimize the difference between experimental data and the values provided by Eq. (17) and to find C_1 and C_2. Then, the lift-curve slope $C_{L\alpha} = dC_L/d\alpha|_{\alpha=0} = C_1$, the maximum lift coefficient $C_{L\max} = -0.25C_1^2/C_2$, and corresponding angle of attack $\alpha_{\max} = -0.5C_1/C_2$ are found. These values are presented in Table 4 for all curves in Figs. 12 and 13.

The lift-curve slope is of primary importance for the performance of flapping-wing aircraft. Note that, for a given value of the advance ratio J, the lift-curve slope for the 74 cm wing is up to 22% higher than for the 25 cm wing. A similar effect is observed with the maximum lift coefficient.

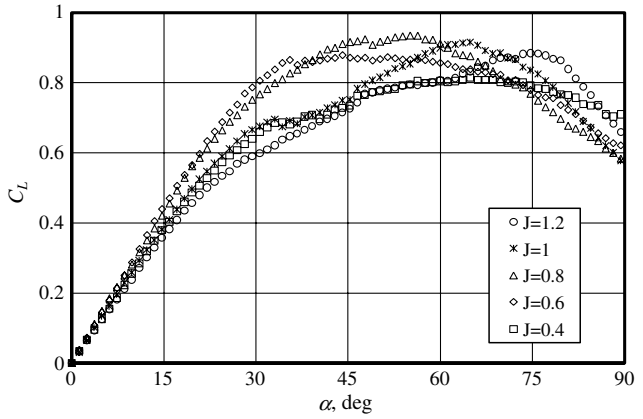

Fig. 12 Variation of lift coefficient with angle of attack and advance ratio (74 cm wing).

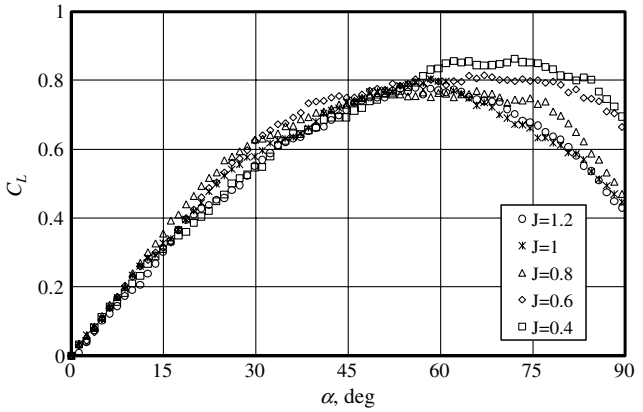

Fig. 13 Variation of lift coefficient with angle of attack and advance ratio (25 cm wing).

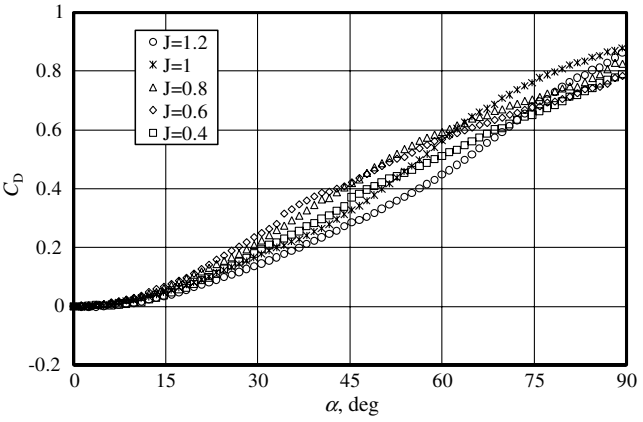

Fig. 14 Variation of drag coefficient with angle of attack and advance ratio (74 cm wing).

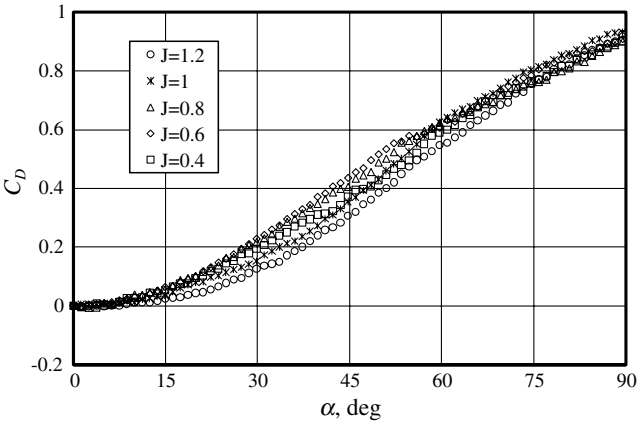

Fig. 15 Variation of drag coefficient with angle of attack and advance ratio (25 cm wing).

The drag coefficient curve is approximated by a cubic polynomial:

$$C_D = K_2\alpha^2 + K_3\alpha^3 \tag{18}$$

Coefficients of Eq. (18) are provided in Table 5 for both wings. For a given J, the maximum drag coefficient and coefficient K_2 are higher for the 25 cm wing. No single trend is seen for K_3, though.

Lift and drag coefficients were averaged over the advance ratio J for each angle of attack. Approximations, Eqs. (17) and (18), were constructed for the 74 and 25 cm wings, and their coefficients are

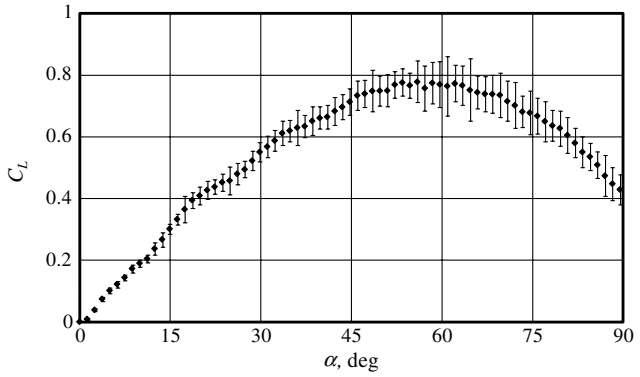

Fig. 16 Lift coefficients with error bars for 25 cm wing at $J = 1.2$ (25 cm wing).

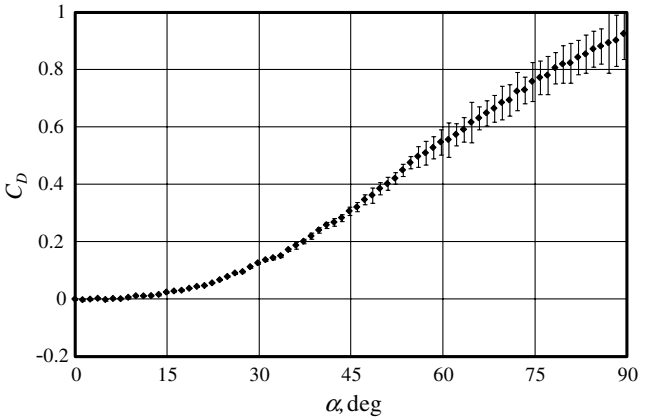

Fig. 17 Drag coefficients with error bars for 25 cm wing at $J = 1.2$ (25 cm wing).

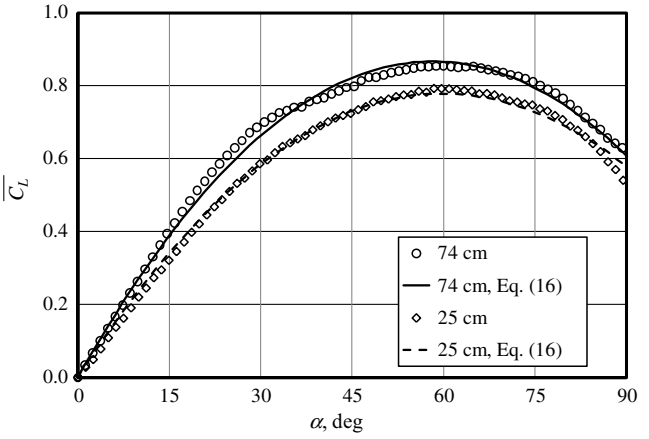

Fig. 18 Variation of average lift coefficient with angle of attack.

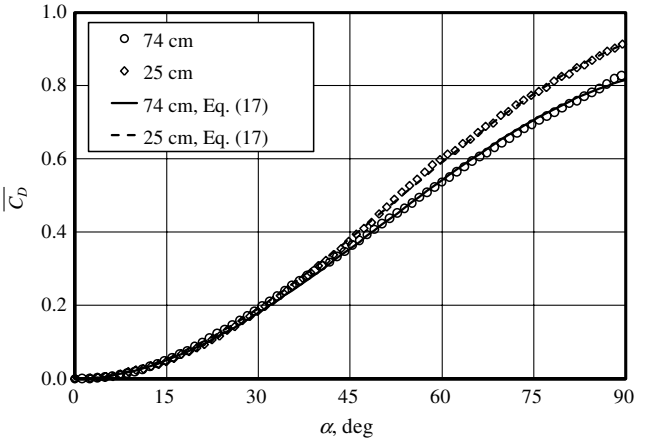

Fig. 19 Variation of average drag coefficient with angle of attack.

provided in Tables 4 and 5, respectively. Plots of the lift coefficient $\bar{C}_L$ and the drag coefficient $\bar{C}_D$ averaged over J are shown in Figs. 18 and 19, respectively. These approximations are found to be valid with the regression coefficient of $R^2 > 0.99$. Overall, averaged experimental data are less scattered. The maximum average lift coefficient is higher in the 72 cm wing by about 10% and, contrary, the maximum drag coefficient is higher in the 25 cm wing by about 10%. There is a rather small difference between drag coefficients for the 25 and 74 cm wings, especially for angles of attack smaller than 45 deg.

Table 4 Lift-curve parameters

Wing model	25 cm				74 cm			
J	Re	$C_{L\alpha}$	$C_{L\max}$	$\alpha_{\max}$	Re	$C_{L\alpha}$	$C_{L\max}$	$\alpha_{\max}$
0.4	24,290	0.0235	0.829	70.4	56,100	0.0267	0.830	62.0
0.6	26,300	0.0259	0.822	63.3	60,750	0.0333	0.914	54.8
0.8	28,900	0.0274	0.782	56.9	66,700	0.0341	0.924	54.1
1	31,950	0.0272	0.755	55.5	73,700	0.0292	0.861	58.8
1.2	35,200	0.0260	0.739	56.7	81,300	0.0260	0.838	65.5
J-averaged		0.0260	0.779	59.8		0.0298	0.869	58.3

Table 5 Drag-curve approximation coefficients

Wing model	25 cm				74 cm			
J	Re	$K_2 \cdot 10^4$	$K_3 \cdot 10^6$	$C_{D\max}$	Re	$K_2 \cdot 10^4$	$K_3 \cdot 10^6$	$C_{D\max}$
0.4	24,290	2.63	−1.68	0.89	56,100	2.44	−1.66	0.77
0.6	26,300	3.11	−2.24	0.88	60,750	3.09	−2.43	0.72
0.8	28,900	3.02	−2.17	0.86	66,700	3.02	−2.27	0.78
1	31,950	2.52	−1.47	0.96	73,700	2.35	−1.36	0.91
1.2	35,200	2.00	−0.90	0.95	81,300	1.67	−0.65	0.88
J-averaged		2.66	−1.70	0.91		2.51	−1.67	0.81

VI. Conclusions

Aerodynamic force measurements were conducted in the University of Arizona wind tunnel using 25 and 74 cm flapping-wing models. The effects of angle of attack, advance ratio, and wing size on stroke-averaged aerodynamic forces and coefficients were analyzed. Stroke-averaged lift and horizontal force were measured at the angle of attack varied from 0 deg (horizontal position) to 90 deg (vertical position).

1) The results showed that flapping wings do not exhibit the typical abrupt stall seen with fixed wings. The nonstalling mechanism in flapping wings makes use of high dynamic pressure on the advancing stroke, which prevails over the lowering or even negative dynamic pressure on the retreating stroke.

2) With an advance ratio increase, the lift increases. When the flapping axis becomes vertical, the lift magnitude is higher than the propulsive thrust for hovering at zero freestream velocity.

3) These results have significant implications for the performance of flapping-wing apparatus. The smoothness of the lift curve over the range of the angle of attack from the horizontal to the vertical is a necessary condition for a smooth transition from a level flight to a hover and back. In the case of a sudden increase of the wind speed, the lift increases pushing a flapping wing safely off the ground.

4) It was found that, for a given advance ratio, values of angles of attack corresponding to the balance of the thrust and the drag forces are close in both wings. The balanced angle decreases exponentially with advance ratio. Note that the balanced angle can be effectively used in predictions of the performance of flapping-wing vehicles in level, steady flight.

5) The problem of the selection of a characteristic velocity was addressed using obtained experimental data for aerodynamic forces and a criterion of the minimum coefficient of variation. The thrust, lift, and drag coefficients were defined using a vector sum of freestream velocity and mean flapping velocity of the wing tip as a characteristic velocity.

6) The effects of advance ratio and wing size on aerodynamic coefficients in flapping wings were discussed. The maximum average lift coefficient was higher in the 72 cm wing by about 10% and, contrary, the maximum drag coefficient was higher in the 25 cm wing by about 10%.

Acknowledgments

This project was sponsored by grant FA9550-10-1-0452 from the U.S. Air Force Office of Scientific Research (Douglas Smith, Program Manager). The authors also would like to thank Gunjan Maniar for his contributions to this work and Gregg Abate for fruitful discussions provided.

References

[1] Mueller, T. J., and DeLaurier, J. D., "An Overview of Micro Air Vehicle Aerodynamics," *Fixed and Flapping Wing Aerodynamics for Micro Air Vehicle Applications*, edited by T. J. Mueller, Vol. 195, AIAA, Reston, VA, 2001, pp. 1–12.

[2] Keennon, M., and Grasmeyer, J., "Development of Two MAVs and a Brief Vision for the Future of MAVs Design," AIAA International Air and Space Symposium and Exposition: The Next 100 Years, Dayton, OH, AIAA Paper 2003-2901, July 2003.

[3] DeLaurier, J. D., "Ornithopter Research," *2003 Bioflight Workshop*, NASA Langley Research Center, Hampton, VA, Aug. 2003.

[4] Krashanitsa, R., Silin, D., Shkarayev, S., and Abate, G., "Flight Dynamics of a Flapping-Wing Air Vehicle," *International Journal of Micro Air Vehicles*, Vol. 1, No. 1, 2009, pp. 35–49. doi:10.1260/1756-8293.1.1.35

[5] Sane, S. P., "Review. The Aerodynamics of Insect Flight," *Journal of Experimental Biology*, Vol. 206, No. 2003, pp. 4191–4208. doi:10.1242/jeb.00663

[6] Rozhdestvensky, K. V., and Ryzhov, V. A., "Aerodynamics of Flapping-Wing Propulsors," *Progress in Aerospace Sciences*, Vol. 39, No. 8, 2003, pp. 585–633. doi:10.1016/S0376-0421(03)00077-0

[7] Shyy, W., Berg, M., and Ljungqvist, D., "Flapping and Flexible Wings for Biological and Micro Air Vehicles," *Progress in Aerospace Sciences*, Vol. 35, No. 5, 1999, pp. 455–505. doi:10.1016/S0376-0421(98)00016-5

[8] Taylor, G. K., "Mechanics and Aerodynamics of Insect Flight Control," *Biological Reviews of the Cambridge Philosophical Society.* Vol. 76, No. 4, 2001, pp. 449–471.

[9] Ansari, S. A., Zbikowski, R., and Knowles, K., "Aerodynamic Modeling of Insect-Like Flapping Flight for Micro Air Vehicles," *Progress in Aerospace Sciences*, Vol. 42, No. 2, 2006, pp. 129–172. doi:10.1016/j.paerosci.2006.07.001

[10] Shyy, W., Lian, Y., Tang, J., Liu, H., Trizila, P., Stanford, B., Bernal, L., Cesnik, C., Friedmann, P., and Ijfu, P., "Computational Aerodynamics of Low Reynolds Number Plunging, Pitching and Flexible Wings for MAV Applications," 46th AIAA Aerospace Sciences Meeting and Exhibit, Reno, NV, AIAA Paper 2008-523, 7–10 Jan. 2008.

[11] van den Berg, C., and Ellington, C. P., "The Vortex Wake of 'Hovering' Model Hawkmoth," *Philosophical Transactions: Biological Sciences*, Vol. 352, No. 1351, 1997, pp. 317–328. doi:10.1098/rstb.1997.0023

[12] van den Berg, C., and Ellington, C. P., "The Three-Dimensional Leading-Edge Vortex of a "Hovering" Model Hawkmoth," *Philosophical Transactions: Biological Sciences*, Vol. 352, No. 1351, 1997, pp. 329–340. doi:10.1098/rstb.1997.0024

[13] Dickinson, M. H., "The Effects of Wing Rotation on Unsteady Aerodynamic Performance at Low Reynolds Numbers," *Journal of Experimental Biology*, Vol. 192, 1994, pp. 179–206.

[14] Dickinson, M. H., Lehmann, F.-O., and Sane, S. P., "Wing Rotation and the Aerodynamic Basis of Insect Flight," *Science*, Vol. 284, No. 5422, Jun. 1999, pp. 1881–2044. doi:10.1126/science.284.5422.1954

[15] Singh, B., and Chopra, I., "Insect-Based Hover-Capable Flapping Wings for Micro Air Vehicles: Experiments and Analysis," *AIAA Journal*, Vol. 46, No. 9, Sept. 2008, pp. 2115–2135. doi:10.2514/1.28192

[16] Gallivan, P., and DeLaurier, J., "An Experimental Study of Flapping Membrane Wings," *Canadian Aeronautics and Space Journal*, Vol. 53, No. 2, June 2007, pp. 35–46. doi:10.5589/q07-005

[17] Ellington, C. P., "The Aerodynamics of Hovering Flight. 6. Lift and Power Requirements," *Philosophical Transactions of the Royal Society of London, Series B: Biological Sciences*, Vol. 305, No. 1122, 1984, pp. 145–181. doi:10.1098/rstb.1984.0054

[18] Ellington, C. P., "The Novel Aerodynamics of Insect Flight: Applications to Micro-Air Vehicles," *Journal of Experimental Biology*, Vol. 202, 1999, pp. 3439–3448.

[19] Ol, M., Parker, G., Abate, G., and Evers, J., "Flight Controls and Performance Challenges for MAVs in Complex Environments," AIAA Guidance, Navigation and Control Conference and Exhibit, Honolulu, AIAA Paper 2008-6508, 18–21 Aug. 2008.

[20] Aki, M., Waszak, M., and Shkarayev, S. V., "Development of Micro Air Vehicles with In-Flight Adaptive Wing," *Introduction to the Design of Fixed-Wing Micro Air Vehicles Including Three Case Studies*, edited by T. J. Mueller , J. C. Kellogg, P. G. Ifju, and S. V. Shkarayev, AIAA Education Series, AIAA, Reston, VA, 2007, pp. 241–275, Chapter 6.

[21] Maniar, G., Randall, R., Shkarayev, S., Goff, Z., and Beran, P., "Kinematics of Free-Flight Ornithopters," 50th AIAA Aerospace Sciences Meeting including the New Horizons Forum and Aerospace Exposition, Nashville, TN, AIAA Paper 2012-0666, Jan. 2012, p. 18.

[22] Shkarayev, S., Maniar, G., and Shekhovtsov, A. V., "Experimental and Computational Modeling of the Kinematics and Aerodynamics of Membrane Flapping Wings," 50th AIAA Aerospace Sciences Meeting including the New Horizons Forum and Aerospace Exposition, Nashville, TN, AIAA Paper 2012-1208, 9–12 Jan. 2012, p. 45.

[23] Shkarayev, S., and Silin, D., "Applications of Actuator Disk Theory to Membrane Flapping Wings," *AIAA Journal*, Vol. 48, No. 10, Oct. 2010, pp. 2227–2234. doi:10.2514/1.J050139

[24] Glauert, H., "A General Theory of Autogyro," *Research and Memoranda No. 1111*, Scientific Research Air Ministry, 1926, pp. 558–593.

[25] Ellington, C. P., "The Aerodynamics of Hovering Insect Flight 5: A Vortex Theory," *Philosophical Transactions of the Royal Society of London, Series B: Biological Sciences*, Vol. 305, No. 1122, 1984, pp. 115–144. doi:10.1098/rstb.1984.0053

C. Cesnik
Associate Editor